Determination of ^{39}K scattering lengths using photoassociation spectroscopy of the 0_g^- state

James P. Burke, Jr.,* Chris H. Greene, and John L. Bohn
JILA and the Department of Physics, University of Colorado, Boulder, Colorado 80309-0440

H. Wang, P. L. Gould, and W. C. Stwalley
Department of Physics, University of Connecticut, Storrs, Connecticut 06269-3046

(Received 25 May 1999)

Threshold scattering properties of ^{39}K atoms are extracted from a line-shape analysis of photoassociation data. Specifically, we consider the rovibrational levels ($v'=0-6$) populated in the photoassociation process $K(4S)+K(4S)+\hbar\omega \rightarrow K_2^*[0_g^-(v',J')]$. The measured spectra exhibit several general trends, including large $J'=2$ linewidths, large relative $J'=4$ peak intensities, and odd rotational lines which are weak or missing. The even J' features signal the presence of a *d*-wave shape resonance in the ground-state collisions. The combination of spectral features allows us to place the following limits on the ground-state singlet and triplet scattering lengths, $a_s=140^{+6}_{-9}$ a.u. and $a_t=-17-0.045(C_6-\bar{C}_6)\pm 25$ a.u., $\bar{C}_6=3800$ a.u. [S1050-2947(99)03512-X]

PACS number(s): 32.70.−n, 32.80.Pj, 33.15.Pw, 33.20.Vq

I. INTRODUCTION

Since the first realization of Bose-Einstein condensation (BEC) in a dilute gas of Rb atoms [1] three years ago, researchers have performed an impressive array of experiments probing the dynamics and physical characteristics of such condensates. This experimental impetus has led to a large body of theoretical work devoted to the analysis of present (and future) experiments. Although the theoretical techniques employed to describe the underlying physics have been quite diverse, they are connected by a common thread. That is, the effective interaction between particles in the condensate is modeled using the two-body *s*-wave scattering length *a*. Knowledge of this single collision parameter *a* (and of course experimental trap parameters) has allowed theorists to successfully describe a multitude of experimental observations such as excitation frequencies, size [2], and rate of formation [3] of the condensates.

Unfortunately, *ab initio* calculations of the two-body molecular interactions have proved unable to determine sensitive quantities such as the scattering length to sufficient accuracy. To date, it has only been through the collaboration of experiment and theory that *a* has been established with reasonable precision. Photoassociation (PA) spectroscopy [4] has proven to be an extremely useful tool in this regard. For example, the scattering lengths are known quite accurately for Li [5], Na [6], Rb [7], and to a lesser extent Cs [8] primarily through the analysis of PA experiments. Notably absent from this list is potassium, an omission which is addressed now in this article. An independent analysis of the ^{39}K 1_u spectrum also addresses this situation [9].

Photoassociation is the process by which an excited molecular bound state is resonantly formed during the collision of two free atoms through photoexcitation, e.g., with a CW laser. In our case, we consider two ^{39}K atoms in their $4S$ ground states colliding in the presence of a weak laser field that excites them to a rovibrational bound level of the electronically excited 0_g^- state whose dissociation limit is the $4S+4P_{3/2}$ threshold. The 0_g^- adiabatic potential curve is created by a long range avoided crossing between a repulsive $^3\Pi_g$ state dissociating to the $4S+4P_{1/2}$ threshold and an attractive $^3\Sigma_g^+$ state dissociating to the $4S+4P_{3/2}$ threshold [10,11]. The inner wall of the 0_g^- potential in K_2 lies at an internuclear separation $R\sim 40$ a.u. Such a large inner turning point implies that the electronic wave functions of the two atoms do not overlap significantly and thus the excited state potential, as well as the molecular dipole matrix elements, can be determined solely from atomic parameters which are known quite accurately. In addition, the rovibrational wave functions used in this analysis span a range of internuclear separations from 40–80 a.u. (see Fig. 1). An investigation of the spectroscopic line shapes and relative intensities will therefore provide information on the ground-state wave functions over this same range via the free-bound Franck-Condon factors. Determination of the nodal pattern of the ground-state *s*-wave function over this range of *R* generally suffices to predict the two-body scattering length *a* accurately.

Previous estimates of K scattering lengths have appeared in the literature [12,13]. However, in both cases the work was based on conventional molecular spectroscopy [14,15] which provided information on the ground-state potentials only over the range $R=5-30$ a.u. In addition, the last measured bound state was approximately 1.7 cm^{-1} below the $4S+4S$ threshold, too low to extrapolate reliably to threshold. The analysis presented in this paper makes use of both the conventional spectroscopic data as well as the new PA experimental data and thus provides a more reliable prediction for the K scattering lengths.

II. EXPERIMENTAL PROCEDURE

The experimental setup has been described in detail elsewhere [16,17]. However, we provide here a brief description for completeness. In particular, we focus on the experimental

*Present address: National Institute of Standards and Technology, Gaithersburg, MD 20899-8423.

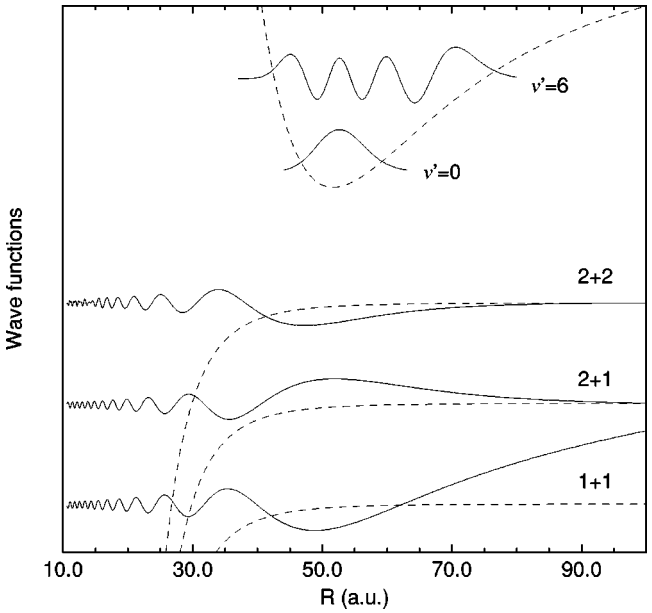

FIG. 1. Schematic of the ground- and excited-state potentials (dashed lines) and wave functions (solid lines). The ground-state thresholds are labeled by their f_a+f_b quantum numbers. The ground-state wave functions were calculated at zero energy relative to the 1+1 threshold. The excited state wave functions correspond to the lowest and highest vibrational levels ($v'=0$ and 6, respectively) used in the analysis. The graph is not to scale.

checks taken to ensure the quality of the data.

A sample of 10^7 ^{39}K atoms, density $>10^{11}$ atoms/cm^3 at a temperature of ~ 400 μK are prepared in a ''dark spot'' vapor cell magneto-optical trap (MOT). The atoms are trapped predominately in their $f_a=1$ hyperfine state ($\vec{f}_a=\vec{s}_a+\vec{i}_a, i_a=3/2$). Separate single-mode tunable ring Ti:sapphire lasers (Coherent CR 899-29) provide the trapping beams and induce the PA transitions. The total output power of the trapping laser is ~ 300 mW at 766.5 nm while the PA laser intensity is typically 50 mW/cm^2. The analysis presented below concentrates on the $v'=0-6$ vibrational levels of the 0_g^- state. For these low lying states, trap loss spectra are not easily observed because the local kinetic energy is not large enough to allow atoms to escape from the trap when the excited vibrational state decays through bound-free spontaneous emission of a photon. Detection of the PA resonances is therefore obtained by recording ion production after a double-resonance transition from the 0_g^- rovibrational state to an autoionizing 1_u state below the highly excited $4S+nD$ ($n=5$ or 6) asymptote [19]. In particular, a tunable ring dye laser (Coherent CR899-29, operated with R110 or R6G dyes) provides the second photon, at frequency ω_2 and typical intensity 12 W/cm^2, for the double-resonance process and a channeltron multiplier records the subsequent production of ions. More details about the high-resolution PA spectroscopy of the 0_g^- state can be found in Ref. [17].

Several measures have been taken to ascertain the influence of light at ω_2 on the PA spectrum of the 0_g^- state. First, spectra have been recorded using final autoionizing states below both the $4S+5D$ and $4S+6D$ asymptotes. Representative examples of these spectra are shown in Fig. 2. These

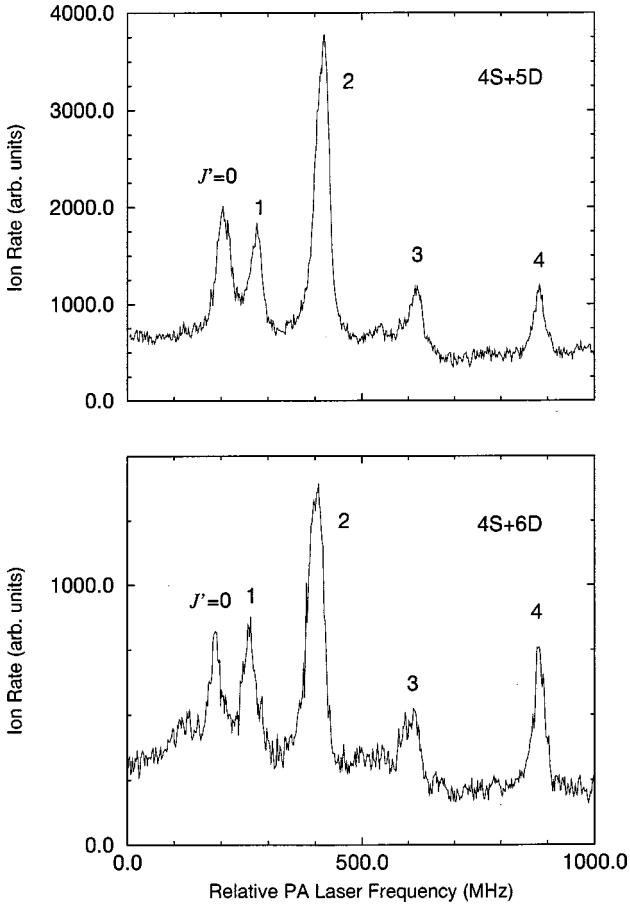

FIG. 2. Representative examples of the 0_g^- $v'=0$ spectra obtained using autoionizing final states below the $4S+5D$ and the $4S+6D$ thresholds. The rotational assignment J' of each peak is indicated in the graphs.

highly excited final states are structureless and broad [19] with widths ranging from ~ 1 GHz for levels near the $4S+5D$ limit to ~ 2 GHz for levels near the $4S+6D$ asymptote. General trends in the PA spectra of the 0_g^- state, such as, weak or missing odd J' rotational levels, anomalous $J'=2$ linewidths, and large $J'=4$ relative intensities were consistent in both cases. The only noticeable differences occur in the $J'=4$ relative intensity which was typically a factor of 1.5–2 bigger in the spectra observed using final states below the $4S+6D$ limit. This difference is attributed to slightly hotter atoms in the MOT (based on linewidths) and the broader final state.

PA spectra of the 0_g^- state were measured by fixing ω_2 to a $0_g^-(v'J'=2)\rightarrow 1_u(v)$ transition near the $4S+nD$ asymptote, then scanning the PA laser frequency. We found that changing ω_2 by the differences between the $J'=2$ and 0 levels and between the $J'=2$ and 4 levels affected only the $J'=4$ relative intensity by roughly a factor of 1.5 while preserving all other trends in the data (see for example Fig. 3). Changing the power at ω_2 only affected the total ion production rate. In addition, we varied the PA laser intensity by a factor of 2 and observed no noticeable power broadening.

III. THEORY

A previous analysis of the ^{23}Na 0_g^- spectrum [6] has shown that two color photoassociation line shapes can be

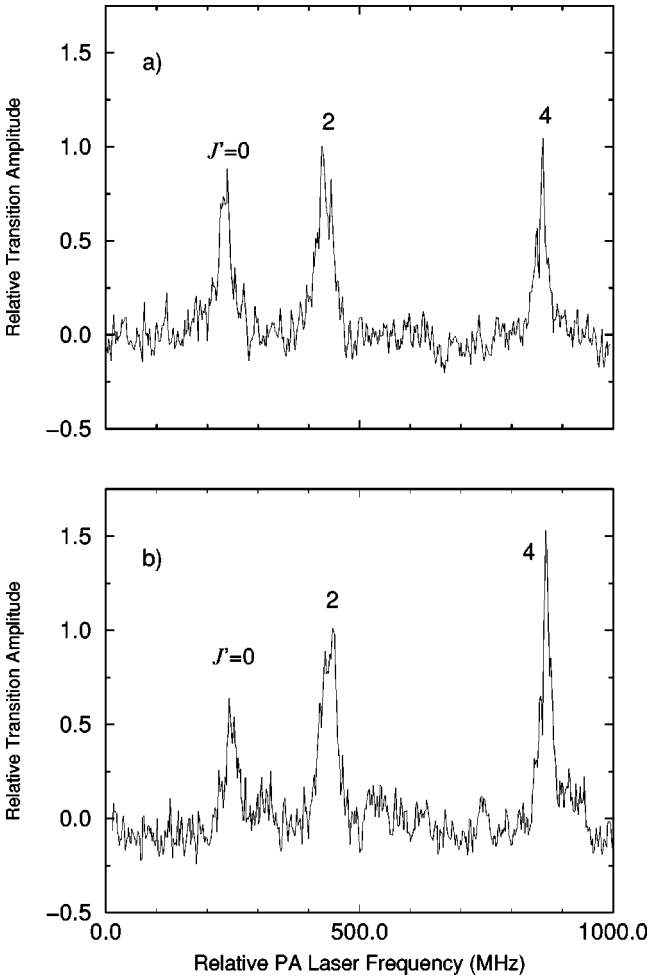

FIG. 3. Representative examples of the 0_g^- $v'=3$ rotational spectra obtained for different values of ω_2. The relative transition amplitude is dimensionless. (a) ω_2 fixed to a $0_g^-(J'=2)\rightarrow 1_u(v)$ transition near the $4S+6D$ asymptote. (b) ω_2 fixed to a $0_g^-(J'=4)\rightarrow 1_u(v)$ transition near the $4S+6D$ asymptote.

accurately modeled by explicitly considering the first PA step alone provided the second transition is to a broad, structureless final state. For a cloud of atoms at temperature T, and an angular laser frequency ω, the expected free-bound transition signal is given by [6,20]

$$S(v',J',\omega,T)=\eta\sum_{\beta' p' f l p \alpha} n_f(2l+1) \times\int_0^\infty dE\,\frac{e^{-E/k_BT}|\langle\phi_{p'\beta'}^{v'J'}|\hbar\Omega|\Psi_{flp\alpha}^{E}\rangle|^2}{(E+\hbar\omega-E^{v'J'})^2+(\gamma/2)^2}. \tag{1}$$

The structure of this expression is as follows: A resonance denominator describes the transition from an incident continuum energy E to the bound state energy $E^{v'J'}$ and incorporates the excited state's radiative linewidth γ. We assume that the second laser at ω_2 and hyperfine structure contribute negligibly to the observed linewidth. These assumptions should be reasonable considering the low laser power involved and small hyperfine splittings [21]. We have therefore taken $\gamma=12$ MHz which is simply twice the atomic natural linewidth [10,22]. The numerator in Eq. (1) contains a squared dipole matrix element that determines the strength of each resonant transition. The resonant rates include an average over all initial states, a thermal average over incident energy and a sum over all unresolved final states. In addition, we insert a factor η to represent the efficiency with which the probe laser at ω_2 makes observable products. For the present analysis, we assume η is independent of the intermediate quantum numbers v', J'. As discussed in the experimental section, this approximation is not strictly valid which leads to an increase in our final fit uncertainties.

In more detail, the excited bound state wave function ϕ is labeled by its vibrational quantum number v', rotational quantum number J', parity p', and β' to represent all other quantum numbers needed to define the wave function uniquely (including nuclear spin degrees of freedom). The experiment did not resolve any hyperfine structure in the spectra and therefore the excited state nuclear spin degrees of freedom are simply summed over. The ground-state wave function of the two colliding atoms Ψ is labeled by f, the total spin angular momentum of the pair, l the mechanical rotation (sometimes denoted as the partial wave), the parity p, and α represents all other quantum numbers needed to uniquely define the quantum state. Here, f denotes the vector sum of each atom's total spin angular momentum, $\vec{f}=\vec{f}_a+\vec{f}_b$ where a and b label each atom. The collision energy is defined as E. The ground and excited states are coupled by the electronic dipole operator represented by $\hbar\Omega$. The final quantity to be defined is n_f which represents the population of atoms in the collision entrance channel f. For a randomly polarized gas of identical particles, this weight is given by $n_f=(2f+1)/N_{\{f_a,f_b\}}$ where $N_{\{f_a,f_b\}}=(2f_a+1)(2f_b+1+\delta_{f_a,f_b})/(1+\delta_{f_a,f_b})$ is the total number of distinct symmetrized spin channels. It should be noted that averaging the dipole matrix elements over initial states cancels both the $2f+1$ factor above and the $2l+1$ factor in Eq. (1). The exact form of Eq. (1) is slightly different than that given in Ref. [9]. This is simply the result of using a different angular momentum coupling scheme and, in fact, the two equations are equivalent.

A. Excited state

Radial wave functions for the ground and excited states are key quantities required for the evaluation of Eq. (1). We begin with a discussion of the excited state. The excited-state potential can be described to first order by the simple analytical model of Movre and Pichler [10,23]. It has been shown [24,25] that for the lowest few vibrational levels the bound state energies can be calculated quite accurately by simply including higher order corrections to this model. Since we are considering only $v'=0$–6 in our analysis, this approximate description of the potential will suffice.

We generate the $^{39}K_2$ 0_g^- adiabatic potentials following the method outlined in Ref. [17]. The 2×2 Hamiltonian which describes the $\Omega=0$ Hund's case c states is given in a Hund's case a representation $(^3\Pi_g,{}^3\Sigma_g^+)$ by

TABLE I. The excited-state long-range dispersion coefficients used in this work [Eq. (3)] are taken from Ref. [17]. The coefficients are given in atomic units.

Coefficient	Π	Σ
C_3	−8.436	16.872
C_6	6272	9365
C_8	762 300	1 975 000

$$\underline{H}=\begin{pmatrix} V_\Pi+V_\Pi^R-\frac{\Delta}{3} & \frac{\sqrt{2}}{3}\Delta \\ \frac{\sqrt{2}}{3}\Delta & V_\Sigma+V_\Sigma^R \end{pmatrix}, \tag{2}$$

where $\Delta=57.706\ \mathrm{cm}^{-1}$ represents the atomic spin-orbit splitting. The electrostatic molecular interaction $V_{\Lambda'}$ is accurately represented for large R by a multipole expansion with the coefficients given in Table I:

$$V_{\Lambda'}=-f^{\Pi/\Sigma}\frac{C_3^{\Pi/\Sigma}}{R^3}-\frac{C_6^{\Pi/\Sigma}}{R^6}-\frac{C_8^{\Pi/\Sigma}}{R^8}. \tag{3}$$

Retardation effects are incorporated into $f^{\Pi/\Sigma}$. These have the form [18]

$$f^{\Pi}=\cos(R/\lambda)+(R/\lambda)\sin(R/\lambda)-(R/\lambda)^2\cos(R/\lambda),$$

$$f^{\Sigma}=\cos(R/\lambda)+(R/\lambda)\sin(R/\lambda). \tag{4}$$

Here, $\lambda=\lambda_{4S\to 4P}/2\pi$ is the transition wavelength. We use an approximate rotational Hamiltonian, including only the diagonal matrix elements $V_{\Lambda'}^R$ which are given by [26]

$$V_\Pi^R=\frac{\hbar^2}{2\mu R^2}[J'(J'+1)+2],$$

$$V_\Sigma^R=\frac{\hbar^2}{2\mu R^2}[J'(J'+1)+4]. \tag{5}$$

The off-diagonal terms are negligible for the low-lying vibrational levels.

The J' dependent 0_g^- potentials $V^{J'}$ are obtained by first diagonalizing Eq. (2) and then adding nonadiabatic diagonal corrections [27]. Bound state energies $E^{v'J'}$ and single channel wave functions $\chi^{v'J'}(R)$ are now easily obtained in the potentials $V^{J'}$. The radial part of the excited state wave function $\phi^{v'J'}(R)$ is then written as an R-dependent linear combination of the two Hund's case a basis functions

$$\phi^{v'J'}(R)=\sum_{\Lambda'} b_{\Lambda'}^{J'}(R)\chi^{v'J'}(R), \tag{6}$$

where $b^{J'}(R)$ is the eigenvector obtained from the diagonalization of Eq. (2).

B. Ground state

Construction of the ground-state potentials begins with singlet [15] and triplet [14] adiabatic Born-Oppenheimer potentials derived from spectroscopic data. The spectroscopic potentials are matched smoothly onto a long range potential which includes long range spin exchange [12] and dispersion [28] contributions. Our final singlet and triplet potentials support 86 and 27 bound vibrational states, respectively, for $^{39}K_2$. We vary the zero energy phase shifts of these potentials by adding a small correction to the inner walls [6]

$$\Delta V(R)=\begin{cases} C_S\tan^{-1}\left[\left(\frac{R-R_e}{\Delta R}\right)^2\right], & R<R_e, \\ 0, & R>R_e. \end{cases} \tag{7}$$

Here $S=0$ or 1 denotes the total electronic spin, R_e is the minimum of the relevant potential, and ΔR is a width parameter, which we took to be $\Delta R=2$ Bohr. Combining these potentials, which are diagonal in a basis of total electronic spin S, with the atomic hyperfine and mechanical rotation Hamiltonians produces a realistic set of coupled molecular potentials.

In the absence of bias magnetic fields (as in this experiment), total angular momentum, $\vec{F}=\vec{f}+\vec{l}$, is conserved in the collision of two ground-state atoms. Further, neglecting the weak magnetic dipole interaction implies that both $\vec{f}$ and $\vec{l}$ are separately conserved. We can therefore model the dynamics of a cloud ($T\sim 400\ \mu$K) of $f_a=f_b=1$ atoms with five distinct Hamiltonians: $f=0,2$ with $l=0,2$ and $f=1$, $l=1$. The Hamiltonians with $f=1$ and 2 contain a set of three coupled channels with one channel converging to each of the three hyperfine thresholds (denoted as f_a+f_b). The $f=0$ Hamiltonian is a two channel case with the second channel converging to the uppermost (2+2) hyperfine threshold. The (1+1) entrance channel is the only channel open as $R\to\infty$. However, the closed channel components of the multicomponent ground-state wave function cannot be neglected as they can still provide a substantial portion of the radial overlap integral (see Fig. 1).

At this point, one could generate the multicomponent ground-state wave functions by directly integrating the radial Schrödinger equation. However as mentioned, the radial overlap integral contains a coherent sum over open and closed channel components. This is important because the first obvious trend in the spectra is the absence of odd J' peaks for most of the vibrational levels. These nontrivial interferences of the radial wave functions make it difficult to visualize a convenient placement of the nodes which would produce such a suppression in the spectra. In order to gain complete confidence that our final fits to the measured data were unique, we undertook a complete search of singlet/triplet parameter space. The additional computational burden of thermal averaging made direct integration extremely inefficient. We therefore generated the ground-state wave functions using multichannel quantum defect (MQDT) techniques developed in Ref. [29] (see also Refs. [30–32]).

The MQDT approach allows us to represent the independent solutions of the radial Schrödinger equation $\underline{M}(E,R)$ for $R\geqslant 40$ a.u. in the following manner:

$$\underline{M}(E,R)=\underline{f}_l^0(\epsilon,R)-\underline{g}_l^0(\epsilon,R)\underline{K}^{\rm sr}. \quad (8)$$

Here, $\underline{f}_l^0$ and $\underline{g}_l^0$ are diagonal matrices of energy-analytic reference wave functions evaluated at energies ϵ_i relative to channel i's threshold, $\epsilon_i=E-E_i$. The notation used here assumes the entrance channel threshold defines zero energy. The single channel reference wave functions f_l^0, g_l^0 are described in detail in Ref. [29] but it suffices here to remark that these wave functions are good solutions of the Schrödinger equation in the presence of the long range potential. The correct linear combination of these reference wave functions which satisfy standing wave boundary conditions is controlled by the short range reactance matrix $\underline{K}^{\rm sr}$. To a very good approximation $\underline{K}^{\rm sr}$, which encapsulates all the multichannel physics, is energy independent [29]. For a given singlet and triplet phase shift, we therefore need only solve the coupled Schrödinger equations at a single energy. The energy dependence of the wave functions derives solely from the single channel reference wave functions and these are independent of the singlet and triplet phase shifts.

However, at this point, $\underline{M}$ does not satisfy proper scattering boundary conditions. These can be imposed with the following transformations which incorporate the four long range MQDT parameters $A(E,l)$, $\mathcal{G}(E,l)$, $\eta(E,l)$, and $\beta(E,l)$ described in Ref. [29]. First, we apply an $n\times n_0$ transformation matrix $\underline{B}(E)$ which imposes exponential decay of the wave function in the asymptotically closed channels (i.e., those with $E<E_i$). Here n is the number of channels (which are symmetrized and labeled by f_a, f_b) and for our case n_0, the number of open channels, is simply 1. $\underline{B}(E)$ is given by

$$\underline{B}=\begin{pmatrix} 1 \\ -(\tan\underline{\beta}+\underline{K}_{QQ}^{\rm sr})^{-1}\underline{K}_{QP}^{\rm sr} \end{pmatrix}, \quad (9)$$

where 1 represents an $n_0\times n_0$ identity matrix and $\tan\underline{\beta}$ is a diagonal matrix of negative energy phases. The labels on the short-range reactance matrix represent a partition into open channel (those channels $i\in P$, for which $\epsilon_i>0$) and closed channel (those channels $i\in Q$, for which $\epsilon_i<0$) subspaces. An energy normalization constant $N(E)$ provides the final boundary condition in the open channel and is obtained by equating $\underline{M}\ \underline{B}$ at large R to the ''physical solution'' $M^{\rm phys}$. The derivation of $N(E)$ is given in the Appendix. An energy-normalized real standing-wave radial wave function for the ground-state is then given by

$$\Psi_{fl}^E(E,R)=\underline{M}_{fl}(E,R)\underline{B}_{fl}(E)\,N_{fl}(E). \quad (10)$$

C. Radiative coupling

The final piece of theory needed is the electronic molecular dipole matrix element. As discussed, the atomic electronic wave functions do not overlap significantly at the internuclear separations at which transitions occur. The dipole operator is therefore given as a sum of individual atomic dipole operators $\vec{r}_a+\vec{r}_b$. Representing the molecular electronic orbital as a linear combination of atomic orbitals [33] ensures that only one atom absorbs a photon. We first evaluate the matrix elements in the Hund's case a basis then project the ground-state basis functions onto a separated atom hyperfine basis. As a test of our formulation we have checked that all dipole selection rules are obeyed and that the lifetime of all 0_g^- rotational levels $J', M_{J'}$ are equal to one half the atomic lifetime [22,10]. As a final test that all the pieces of our theory have been integrated properly we have reproduced the Na spectra illustrated in Ref. [6].

IV. RESULTS

We begin the analysis by choosing scattering lengths [i.e., C_S in Eq. (6)] for the singlet and triplet ground-state potentials. From this pair of potentials, a synthetic rotational $J'=0-4$ progression is generated for vibrational levels $v'=0-6$ via Eq. (1). A ''match'' to the measured data requires that the calculated relative intensities and linewidths of a rotational progression within a given v' agree within experimental bounds simultaneously for each vibrational level $v'=0-6$. We assume a constant cloud temperature, estimated to be 400 ± 100 μK, for all vibrational levels. Absolute intensities are quite uncertain, requiring us to normalize each vibrational spectrum to $S_{\rm peak}(J'=2)=1$. In addition, we adjust the absolute PA laser frequency ω such that the blue edge of the synthetic and measured $J'=2$ lines are aligned for each vibrational spectrum. The absolute intensity and absolute frequency are the only two adjustable fit parameters incorporated into the theory.

We used the data obtained from the $4S+6D$ autoionizing final state exclusively in the final determination of the ground-state potentials. The uncertainties associated with the final autoionizing step were better characterized for this data and therefore more precise bounds on scattering lengths could be obtained. The ground-state potentials were then systematically varied such that the singlet and triplet scattering lengths ranged between $\pm\infty$. The search of singlet/triplet phase space combined information on all rotational peak areas and the $J'=2$ linewidth for vibrational levels $v'=0-6$. The uncertainties in these quantities obtained from several scans of the experimental data determined the final bounds placed on the scattering lengths. A comparison of spectra calculated with our ''nominal'' set of potentials is shown in Fig. 4. The $J'=4$ relative intensity is the main discrepancy between experiment and theory. This can be attributed to optimizing the double resonance experiment using the $J'=2$ intermediate level which then underrepresents the $J'=4$ intensities (see Fig. 3). These searches were conducted for C_6 ranging from 3600–4000 a.u. which is approximately $\pm5\%$ of the nominal value (3813 a.u.) given in Ref. [28]. The final results are given in Table II. The table also translates these results into scattering lengths for other K isotopes. Atomic parameters for each K isotope are listed in Table III.

The analysis of the 0_g^- spectra is simplified somewhat by the following selection rules. The parity of a 0_g^- rotational wave function is $(-1)^{J'+1}$ [6]. The ground-state wave function parity is simply $(-1)^l$. Therefore, dipole selection rules restrict transitions from ground-state collisions in even partial waves l to even rotational levels J' and likewise odd partial waves to odd J''s. More specifically, s-wave collisions contribute to $J'=0,2$, d-wave collisions contribute to $J'=0,2,4$ and p-wave collisions contribute only to $J'=1,3$. In addition the 0_g^- electronic state for like atoms has a

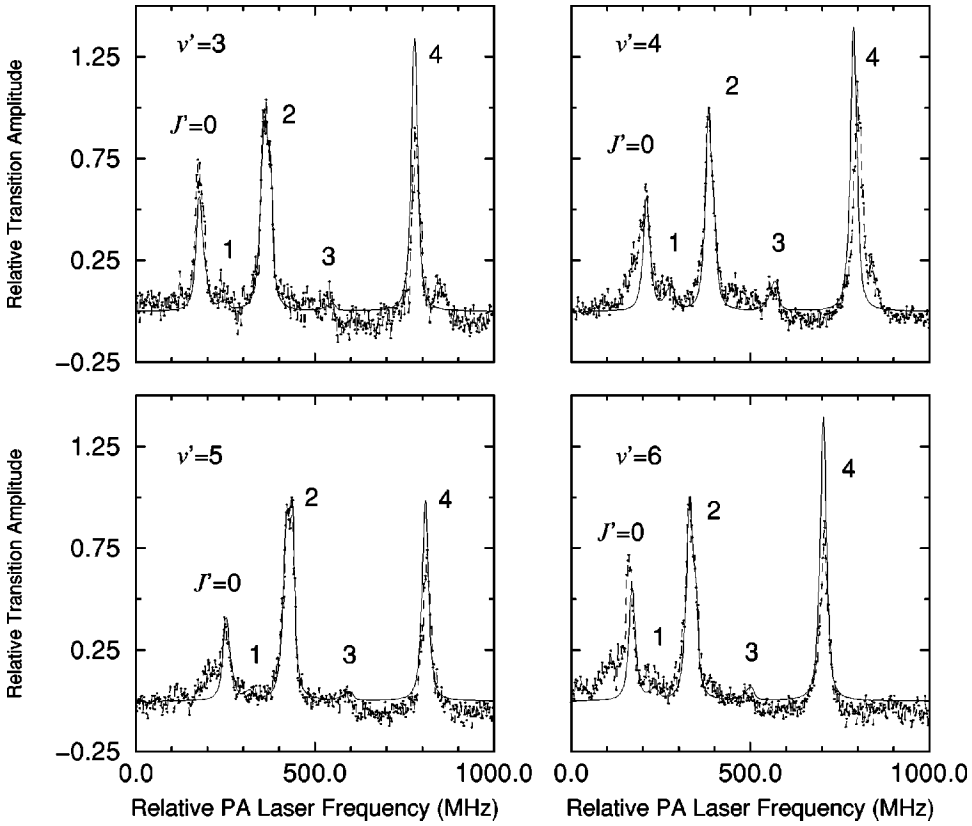

FIG. 4. Comparison of experimental (dashed line) and theoretical (solid line) relative transition amplitudes (dimensionless). The synthetic spectra was calculated using our nominal set of potentials, $a_s = 140$ a.u., $a_t = -17$ a.u., and $C_6 = 3800$ a.u., assuming a cloud temperature of 400 μK. Rotational assignments J' are indicated in each graph. It is believed that the red wing of the $J' = 0$ experimental peaks correspond to additional flux obtained from $f = 1 + f = 2$ collisions. These collisions were not theoretically modeled since they contribute little to the spectrum.

nuclear permutation symmetry which requires $(-1)^{J'+I'}$ to be odd, where I' denotes the quantum number associated with the total nuclear spin $\vec{I} = \vec{i}_a + \vec{i}_b$.

The measured spectra show several distinct trends. First, the *p*-wave features are almost entirely missing from all vibrational scans except $v' = 0$ and 2. Second, the relative intensity of the $J' = 4$ (pure *d* wave) peak is found to be quite large in all the scans. This is somewhat surprising since the height of the *d*-wave centrifugal barrier is roughly 1.5 mK and at cloud temperatures around 400 μK one would expect, in the absence of resonances, the *d*-wave features to be suppressed by the Wigner threshold law. Finally, the $J' = 2$ linewidths are quite large ~ 35 MHz compared to the other rotational lines ~ 25 MHz. The analysis of the measured data will focus on these particular features. In the following discussion we generalize somewhat the contributions of each feature to the limits placed on scattering lengths. However, we want the reader to keep in mind that it is only through the combination of these spectral features that a unique parameter region is found on which limits are ultimately placed.

The large $J' = 2$ linewidths are a particularly interesting feature. We find that these linewidths are a result of a broad

TABLE II. Singlet and triplet scattering lengths a (in a.u.) and quantum defects μ (dimensionless) for collisions among different pairs of potassium isotopes assuming a constant $\overline{C_6} = 3800$ a.u. The scattering length is related to the quantum defect through the following formula [29,38]: $a = -C^2 \tan(\pi\mu)/[1 + \mathcal{G}(0)\tan(\pi\mu)]$ where $C^2 = 0.9579(2mC_6)^{1/4}$, m is the reduced mass of the atom-pair and $\mathcal{G}(0) = -1.0039$. The singlet quantum defect uncertainties are $^{+0.019}_{-0.011}$ for each collision pair, independent of the C_6 value. Finally, the uncertainties associated with each triplet quantum defect and its variation with C_6 is given by: $\mu_t = \overline{\mu_t} + 8.0(10^{-5})(C_6 - \overline{C_6})^{+0.04}_{-0.06}$.

Isotopes	a_s	$\overline{\mu_s}$	a_t	$\overline{\mu_t}$
39+39	140^{+6}_{-9}	0.460	-17 ± 25	0.039
40+40	105^{+3}_{-5}	−0.445	194^{+114}_{-35}	0.388
41+41	85 ± 3	−0.366	65^{+13}_{-8}	−0.268
39+40	-1^{+4}_{-8}	0.002	$-460^{+330}_{-\infty}$	0.212
39+41	113 ± 5	−0.474	205^{+140}_{-40}	0.379
40+41	-50^{+9}_{-18}	0.089	104^{+20}_{-11}	−0.441

TABLE III. Mass in ^{12}C amu, nuclear spin i, and ground-state atomic hyperfine splittings of the K isotopes. A negative value of Δ indicates an ''inverted'' hyperfine structure.

Isotope	Mass	i	Δ (MHz)
39	38.963 707	3/2	461.72
40	39.963 999	4	−1285.79
41	40.961 825	3/2	254.01

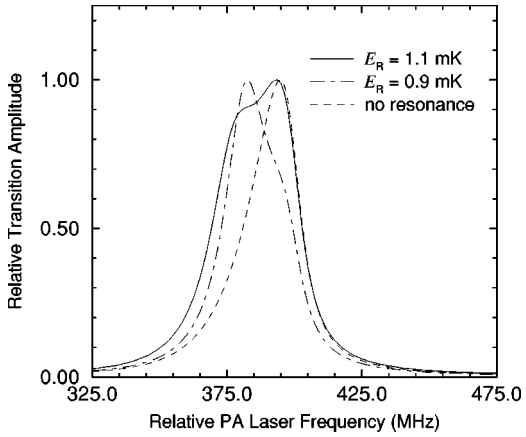

FIG. 5. Comparison of the $J'=2$ linewidths versus the position E_R of the $f=0$ d-wave shape resonance. The no resonance case indicates the s-wave contribution to the linewidth. The position of the resonance controls the relative d-wave contribution to the peak and the amount it is redshifted relative to the s-wave contribution. The relative transition amplitude is dimensionless.

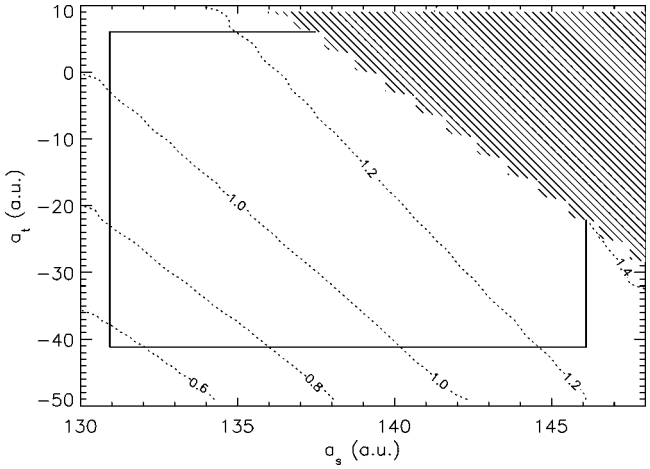

FIG. 6. The dashed lines indicate the energy position E_R given in mK of the d-wave shape resonance in the a_s-a_t plane. The solid rectangle represents our allowed individual singlet and triplet parameter ranges ($C_6=3800$ a.u.) including the ± 100 μK uncertainty in cloud temperature. The hatched region indicates the parameter space excluded by the absence of the $f=2$ g-wave shape resonance.

$f=0$ d-wave shape resonance, at an energy $E_R=1.15 \pm 0.35$ mK with a width $\Delta=0.5\pm 0.2$ mK. The spectral width provides a fairly sensitive probe of the position of the shape resonance. Figure 5 shows the effect on the $J'=2$ linewidth as the position of the shape resonance is varied. As E_R is moved to larger energies, the d-wave contribution to $J'=2$ shifts to the red of the s-wave contribution thereby increasing the overall width of $J'=2$. However, if E_R becomes too large relative to the cloud temperature the thermal averaging suppresses the d-wave intensity contribution effec-

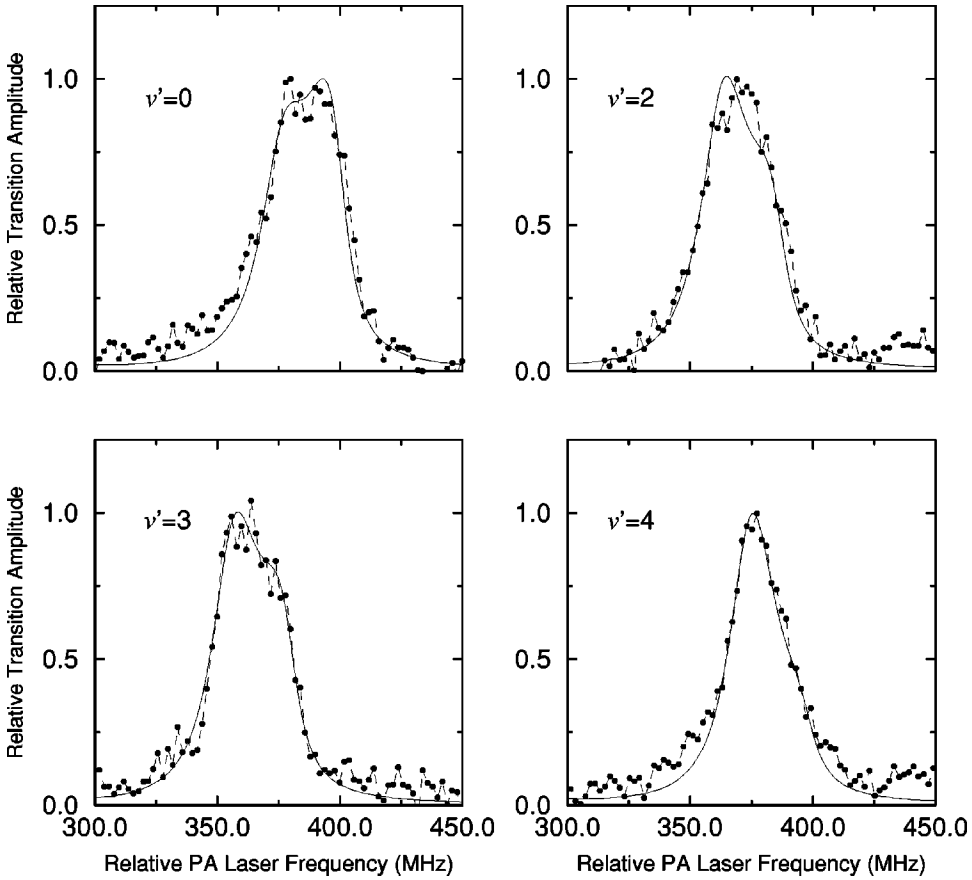

FIG. 7. Comparison of experimental (closed circles) and theoretical (solid line) $J'=2$ linewidths. The synthetic spectra was calculated using our nominal set of potentials, $a_s=140$ a.u., $a_t=-17$ a.u., and $C_6=3800$ a.u., assuming a cloud temperature of 400 μK. Relative transition amplitudes are dimensionless.

tively reducing the linewidth. Similarly, if E_R is moved to smaller energies not only is the red shift reduced but the d-wave contribution with its extra $(2l+1)$ phase space factor [see Eq. (1)] overwhelms the s-wave contribution and again the linewidth is reduced. The large $J'=4$ peaks are also a by-product of this shape resonance and their heights are quite sensitive to the position of the resonance. These constraints force E_R to lie in the range 1.15 ± 0.35 mK creating an ''allowed'' strip in Fig. 6. In particular, the position of the resonance depends sensitively on the singlet scattering length and thus imposes tight bounds on this quantity. However, because the resonance is near the top of the centrifugal barrier and therefore quite broad the spectral linewidths are relatively insensitive to the C_6 value. In fact, we find the bounds on the singlet scattering length are unchanged when C_6 is allowed to vary between 3600–4000 a.u. Allowing a quarter linewidth uncertainty on each $J'=2$ peak, we find the following value for the singlet scattering $a_s=140^{+6}_{-9}$ a.u., which is in good agreement with Ref. [13]. (The bounds on a_s are somewhat more conservative than reported previously in Ref. [34].) Comparison of the $J'=2$ measured linewidths with our ''best'' fit potentials are shown in Fig. 7. Finally, it should be noted that this $f=0$ d-wave shape resonance manifests itself in other features seen in the 1_u spectra [9]. However, we do not agree on the exact position of the resonance and therefore have different constraints on the singlet scattering length. We believe this discrepancy indicates a limitation of the ''naive'' PA theory which disregards the effect of the ionizing laser. This point is discussed in more detail in Ref. [9].

There is, in fact, another bound on E_R. We find that raising E_R above ~1.3 mK introduces an additional $f=2$ g-wave shape resonance [35]. The existence of a g-wave resonance should manifest itself in the 0_g^- spectrum as an additional $J'=6$ peak (as well as contributing to $J'=2$ and 4). However, there is no experimental evidence for an additional rotational peak. Also, the presence of a g-wave resonance would be inconsistent with the 1_u spectra [9]. The exclusion of the g-wave resonance thus reduces slightly our allowed parameter space (see Fig. 6).

Placing bounds on a_t is somewhat more complex. One aspect of this problem is to reproduce the suppression of the p-wave features as was also the case in Na [6]. However, in Na the Franck-Condon overlap was controlled essentially by the wave function in the open channel and therefore a careful placement of a node in this produced the proper cancellation. In our case, the Franck-Condon overlap consists of a coherent sum over the open channel *and* closed channel contributions as emphasized in Fig. 1. The outer turning points of the closed channel potentials occur at roughly the same internuclear separation as the inner turning point of the excited state potential. This of course means that the closed channels, which are on their last half cycle at the Condon point, can have a large effect on the radial overlap integral. Moreover, the shapes of the closed channel wave functions near the Condon point are essentially ''fixed'' in R, as they must begin their exponential decay. Varying the singlet and triplet scattering lengths thus only affects the relative amplitudes in the channels. For example, the amplitudes will be quite small when $a_s\sim a_t$ just as ^{87}Rb spin exchange inelastic rates [36] are suppressed by this criterion. It is therefore not obvious (or unique) where the open channel node needs to be placed in order to reproduce the observed suppression of the p-wave features for all levels except $v'=0$ and 2. However, having already limited the available parameter space by considering the d-wave shape resonance, we find unambiguously that the wave function nodes are bounded as follows: $f=1$, p-wave node is 68^{+9}_{-6} a.u. and the $f=2$, s-wave node is 62^{+4}_{-3} a.u. The positions of these nodes in our allowed a_s-a_t parameter space are controlled almost exclusively by the triplet scattering length. Unfortunately the suppression of the p-wave features is fairly robust in this region which is largely responsible for the bigger uncertainty in the triplet scattering length. Variations in C_6 require a corresponding change in the triplet scattering length to preserve the nodal positions. We found changing the value of the C_6 coefficient simply shifted our allowed parameter region along the triplet axis of the a_s-a_t plane while preserving the area. We have therefore parametrized this dependence in the following manner $a_t=-17-0.045(C_6-\overline{C_6})\pm25$ a.u., $\overline{C_6}=3800$. The two most important scattering lengths for BEC are the triplet scattering length a_t and $f=2$ s-wave scattering length a_{2S}. From our final potentials, we find $a_{2S}=-20-0.055(C_6-\overline{C_6})^{+35}_{-45}$ a.u., in agreement with the results from the 1_u analysis [9].

V. SUMMARY

In conclusion, we have presented a theoretical analysis of the 0_g^- rovibrational spectrum. Comparing the synthetic spectra with the measured relative line intensities and linewidths allowed us to place fairly restrictive bounds on the singlet and triplet s-wave scattering lengths. We have shown that the spectral linewidths indicate the presence of an $f=0$ d-wave shape resonance. However, this resonance did not provide conclusive information on the C_6 coefficient. In addition, the analysis has incorporated the MQDT ideas presented in Ref. [29], which has dramatically improved the efficiency of the theoretical calculations.

Particularly notable in our results is the first accurate determination of a_t for ^{39}K which can be translated into triplet scattering lengths for other isotopic combinations by rescaling the reduced mass. The unfortunately small and probably negative scattering length in ^{39}K poses considerable disadvantages for attaining BEC. The good news is that the ^{41}K triplet scattering length is almost assuredly large and positive and thus this isotope should be a good candidate for BEC. Also, ^{40}K should have a large positive triplet scattering length making the proposition of a mixed-spin state degenerate Fermi gas tangible. We have reported these considerations in detail in a separate study [34]. Our results for both the ^{39}K a_t and a_{2S} scattering lengths are consistent with the analysis of the 1_u spectra [9], and we find our triplet scattering length for ^{40}K is consistent with the value extracted from a recent elastic scattering measurement [37].

ACKNOWLEDGMENTS

We would like to acknowledge useful discussions with E. Tiesinga, C. Williams, and P. Julienne and thank them for providing details of their 1_u work before publication.

This work was supported in part by the National Science Foundation.

APPENDIX

The following transformations and quantities are described in Ref. [29]. We begin with the asymptotic form of the wave function which in our particular case has only a single nonzero component

$$\underline{M}(E,R)\underline{B} \overset{R\to\infty}{\to} f_l^0(E,R) - g_l^0(E,R)\tilde{K}, \tag{A1}$$

where $\tilde{K}$ is given by the following transformation:

$$\tilde{K} = \underline{K}^{\rm sr}_{PP} - \underline{K}^{\rm sr}_{PQ}(\underline{K}^{\rm sr}_{QQ} + \tan\underline{\beta})^{-1}\underline{K}^{\rm sr}_{QP}. \tag{A2}$$

Next we introduce an energy normalized base pair of reference wave functions f,g

$$\begin{pmatrix} f^0(R) \\ g^0(R) \end{pmatrix} = \begin{pmatrix} A^{-1/2} & 0 \\ -A^{-1/2}\mathcal{G} & A^{1/2} \end{pmatrix}\begin{pmatrix} f(R) \\ g(R) \end{pmatrix} \tag{A3}$$

which are phase-shifted relative to spherical Bessel solutions at $R\to\infty$

$$\begin{aligned} f_l(E,R) &\to kR\sqrt{2\mu/\pi k}[j_l(kR)\cos\eta - n_l(kR)\sin\eta], \\ g_l(E,R) &\to kR\sqrt{2\mu/\pi k}[j_l(kR)\sin\eta + n_l(kR)\cos\eta]. \end{aligned} \tag{A4}$$

Here j_l and n_l are the standard spherical Bessel and Neumann functions, μ the reduced mass of the atomic pair and $k=\sqrt{2\mu E}$. The wave function $M' = \underline{M}\ \underline{B}$ at large R can now be written as

$$\begin{aligned} M' \to kR\sqrt{\frac{2\mu}{\pi k}}\left(\frac{\tan\delta^s\cos\eta}{A^{1/2}\tilde{K}}\right)[(1-\tan\delta^s\tan\eta)j_l(kR) \\ -(\tan\delta^s+\tan\eta)n_l(kR)], \end{aligned} \tag{A5}$$

where we have introduced a new phase defined as $\delta^s = \tan^{-1}[A\tilde{K}/(1+\mathcal{G}\tilde{K})]$. We can now determine the normalization constant by simply equating the QDT wave function NM' to the ''physical'' wave function $M^{\rm phys}$ given as $R\to\infty$ by

$$M^{\rm phys} \to kR\sqrt{\frac{2\mu}{\pi k}}[j_l(kR)\cos\delta^p - n_l(kR)\sin\delta^p], \tag{A6}$$

where δ^p is the ''physical'' phase shift and is given in terms of the MQDT parameters by $\delta^p = \delta^s + \eta$. Finally with a little more manipulation, we can write the normalization constant solely in terms of the three long range MQDT parameters $A(E,l)$, $\mathcal{G}(E,l)$, $\beta(E,l)$, and the short range reactance matrix $\underline{K}^{\rm sr}$

$$N(E) = \left(\frac{\sin\delta^s}{A^{1/2}\tilde{K}}\right). \tag{A7}$$

[1] M. H. Anderson, J. R. Ensher, M. R. Matthews, C. E. Wieman, and E. A. Cornell, Science **269**, 198 (1995).

[2] F. Dalfovo, S. Giorgini, L. P. Pitaevskii, and S. Stringari, Rev. Mod. Phys. **71**, 463 (1999), and references therein.

[3] C. W. Gardiner, M. D. Lee, R. J. Ballagh, M. J. Davis, and P. Zoller, Phys. Rev. Lett. **81**, 5266 (1998).

[4] H. R. Thorsheim, J. Weiner, and P. S. Julienne, Phys. Rev. Lett. **58**, 2420 (1987); P. D. Lett, P. S. Julienne, and W. D. Phillips, Annu. Rev. Phys. Chem. **46**, 423 (1995); R. Côté, A. Dalgarno, Y. Sun, and R. G. Hulet, Phys. Rev. Lett. **74**, 3581 (1995).

[5] E. R. I. Abraham, W. I. McAlexander, C. A. Sackett, and R. G. Hulet, Phys. Rev. Lett. **74**, 1315 (1995); E. R. I. Abraham, W. I. McAlexander, J. M. Gerton, R. G. Hulet, R. Côtée, and A. Dalgarno, Phys. Rev. A **53**, R3713 (1996); **55**, R3299 (1997).

[6] E. Tiesinga, C. J. Williams, P. S. Julienne, K. M. Jones, P. D. Lett, and W. D. Phillips, J. Res. Natl. Inst. Stand. Technol. **101**, 505 (1996).

[7] H. M. J. M. Boesten, C. C. Tsai, B. J. Verhaar, and D. J. Heinzen, Phys. Rev. Lett. **77**, 5194 (1996); H. M. J. M. Boesten, C. C. Tsai, J. R. Gardner, D. J. Heinzen, and B. J. Verhaar, Phys. Rev. A **55**, 636 (1997); C. C. Tsai, R. S. Freeland, J. M. Vogels, H. M. J. M. Boesten, B. J. Verhaar, and D. J. Heinzen, Phys. Rev. Lett. **79**, 1245 (1997).

[8] A. Fioretti, D. Comparat, A. Crubellier, O. Dulieu, F. Masnou-Seeuws, and P. Pillet, Phys. Rev. Lett. **80**, 4402 (1998).

[9] C. J. Williams, E. Tiesinga, P. S. Julienne, H. Wang, W. C. Stwalley, and P. L. Gould, Phys. Rev. A **60**, 4427 (1999).

[10] M. Movre and G. Pichler, J. Phys. B **13**, 697 (1980).

[11] W. C. Stwalley, Y.-H. Uang, and G. Pichler, Phys. Rev. Lett. **41**, 1164 (1978).

[12] R. Côté, A. Dalgarno, H. Wang, and W. C. Stwalley, Phys. Rev. A **57**, R4118 (1998).

[13] H. M. J. M. Boesten, J. M. Vogels, J. G. C. Tempelaars, and B. J. Verhaar, Phys. Rev. A **54**, R3726 (1996).

[14] G. Zhao, W. T. Zemke, J. T. Kim, B. Ji, H. Wang, J. T. Bahns, W. C. Stwalley, L. Li, A. M. Lyyra, and C. Amiot, J. Chem. Phys. **105**, 7976 (1996); W. T. Zemke, C. C. Tsai, and W. C. Stwalley, *ibid.* **101**, 10 382 (1994); L. Li, A. M. Lyyra, W. T. Luh, and W. C. Stwalley, *ibid.* **93**, 8452 (1990).

[15] C. Amiot, J. Verges, and C. E. Fellows, J. Chem. Phys. **103**, 3350 (1995); C. Amiot, J. Mol. Spectrosc. **146**, 370 (1991).

[16] H. Wang, P. L. Gould, and W. C. Stwalley, Phys. Rev. A **53**, R1216 (1996).

[17] H. Wang, P. L. Gould, and W. C. Stwalley, J. Chem. Phys. **106**, 7899 (1997).

[18] W. J. Meath, J. Chem. Phys. **48**, 227 (1968).

[19] H. Wang, X. T. Wang, P. L. Gould, and W. C. Stwalley, Phys. Rev. Lett. **78**, 4173 (1997).

[20] R. Napolitano, J. Weiner, P. S. Julienne, and C. J. Williams, Phys. Rev. Lett. **73**, 1352 (1994).

[21] In Ref. [6], hyperfine structure was found to add roughly 2 MHz to the linewidth of the lowest vibrational levels in ^{23}Na whose hyperfine interaction is much larger than ^{39}K.

[22] P. S. Julienne and J. Vigue, Phys. Rev. A **44**, 4464 (1991).

[23] E. I. Dashevskaya, A. I. Voronin, and E. E. Nikitin, Can. J. Phys. **47**, 1237 (1969).

[24] K. M. Jones, P. S. Julienne, P. D. Lett, W. D. Phillips, E. Tiesinga, and C. J. Williams, Europhys. Lett. **35**, 85 (1996).
[25] C. J. Williams, E. Tiesinga, and P. S. Julienne, Phys. Rev. A **53**, R1939 (1996).
[26] H. Lefebvre-Brion and R. W. Field, *Perturbations in the Spectra of Diatomic Molecules* (Academic, New York, 1986).
[27] F. T. Smith, Phys. Rev. **179**, 111 (1969); H. Klar, Phys. Rev. A **15**, 1452 (1977).
[28] M. Marinescu, H. R. Sadeghpour, and A. Dalgarno, Phys. Rev. A **49**, 982 (1994).
[29] J. P. Burke, Jr., C. H. Greene, and J. L. Bohn, Phys. Rev. Lett. **81**, 3355 (1998). We should point out several sign errors in Eqs. (4) and (5) of this reference. The matrix element in row 2 column 1 of Eq. (4) should read $+A^{-1/2}\mathcal{G}$ and in the asymptotic expansion of g in Eq. (5), the last term should read $+n_l(kR)\cos\eta$.
[30] F. H. Mies, J. Chem. Phys. **80**, 2514 (1984); F. H. Mies and P. S. Julienne, *ibid.* **80**, 2526 (1984); F. H. Mies and M. Raoult (unpublished).
[31] B. Gao, Phys. Rev. A **58**, 4222 (1998); **54**, 2022 (1996).
[32] M. J. Cavagnero, Phys. Rev. A **50**, 2841 (1994); M. J. Cavagnero (unpublished).
[33] R. W. Heather and P. S. Julienne, Phys. Rev. A **47**, 1887 (1993).
[34] J. L. Bohn, J. P. Burke, Jr., C. H. Greene, H. Wang, P. L. Gould, and W. C. Stwalley, Phys. Rev. A **59**, 3660 (1999).
[35] E. Tiesinga (private communication).
[36] C. J. Myatt, E. A. Burt, R. W. Ghrist, E. A. Cornell, and C. E. Wieman, Phys. Rev. Lett. **78**, 586 (1997); P. S. Julienne, F. H. Mies, E. Tiesinga, and C. J. Williams, *ibid.* **78**, 1880 (1997); S. J. J. M. F. Kokkelmans, H. M. J. M. Boesten, and B. J. Verhaar, Phys. Rev. A **55**, R1589 (1997); J. P. Burke, Jr., J. L. Bohn, B. D. Esry, and C. H. Greene, *ibid.* **55**, R2511 (1997).
[37] B. DeMarco, J. L. Bohn, J. P. Burke, Jr., M. Holland, and D. S. Jin, Phys. Rev. Lett. **82**, 4208 (1999).
[38] J. L. Roberts, N. R. Claussen, J. P. Burke, Jr., C. H. Greene, E. A. Cornell, and C. E. Wieman, Phys. Rev. Lett. **81**, 5109 (1998).